Journal of Alloys and Compounds 509 (2011) 4569–4573

Contents lists available at ScienceDirect

Journal of Alloys and Compounds

journal homepage: www.elsevier.com/locate/jallcom

Thermodynamics and structural relaxation in Ce-based bulk metallic glass-forming liquids

T. Wang, Y.Q. Yang, J.B. Li, G.H. Rao*

Beijing National Laboratory for Condensed Matter Physics, Institute of Physics, Chinese Academy of Sciences, Beijing 100190, People's Republic of China

ARTICLE INFO

Article history:
Received 8 November 2010
Received in revised form 12 January 2011
Accepted 15 January 2011
Available online 22 January 2011

Keywords:
Metallic glasses
Thermodynamic properties
Glass transition
Structural relaxation

ABSTRACT

Thermodynamics, kinetics and structural relaxation of Ce-based bulk metallic glass-forming liquid were investigated in the glass transition region by calorimetric measurements. The differences in thermodynamic functions were calculated between the supercooled liquid and crystalline state of the Ce-based alloys. Structural relaxation was studied by heating rate dependence of glass transition temperature. In terms of fragility parameter *m*, the Ce-based alloys were stronger liquid than other metallic glass-forming liquids. The correlation of the excellent glass-forming ability of Ce-based alloys with the thermodynamic property (Gibbs free energy) and the kinetic property (*m*) was discussed. The structural relaxation from glass state to the equilibrium supercooled state was well described by Tool–Narayanaswamy–Moynihan (TNM) model using the parameters derived from the calorimetric measurements.

1. Introduction

Bulk metallic glasses (BMGs) have been attracting great attention due to their intriguing physics and promising technological applications [1,2]. The BMGs exhibit an excellent resistance against crystallization and a high thermal stability in supercooled region, which offers a possibility to investigate the relaxation behaviors in the melt far above glass transition temperature T_g. Metallic glass formers can be regarded as dense random packing structure of atoms and are structurally simple in comparison to polymeric, molecular and inorganic glasses. Therefore, the BMGs could be ideal systems for investigating the mechanisms of glass transition and the complex relaxations of supercooled liquids. Thermophysical properties of glass forming liquids are essential for understanding the origins of glass forming ability (GFA) of materials [3–6] and have close correlations with mechanical properties of glasses [7,8]. Thermophysical, mechanical properties and GFA of the metallic glasses are also important for the technological applications of the materials [9,10]. Recently, a family of Ce-based BMGs has been developed [11,12]. The Ce-based BMGs distinguish themselves from other BMGs by their excellent glass-forming ability, exceptionally low glass transition temperature T_g close to room temperature, and superplasticity at low temperature [13]. The mechanical properties of the Ce-based metallic glasses were studied by Zhang et al. [13,14], but detailed analysis of the thermal and kinetic properties of supercooled state and glass transition itself are less reported. In this work, we carried out an investigation of the thermodynamics and kinetics of $Ce_{68}Al_{10}Cu_{20}Co_2$, $Ce_{65}Al_{10}Cu_{20}Co_5$, and $Ce_{60}Al_{10}Cu_{20}Co_{10}$ alloys. The correlation of the glass-forming ability to thermodynamic and kinetic factors was discussed in terms of Gibbs free energy and fragility. The structural relaxation in the glass transition is illustrated by Tool–Narayanaswamy–Moynihan (TNM) model.

2. Experimental

Bulk Ce-based ingots of nominal composition were prepared by arc melting pure Cu (99.99 wt.%), Al (99.99 wt.%), Co (99.9 wt.%) and industrial pure Ce (99.5 wt.%) under a Ti-gettered argon atmosphere. The alloy ingots were remelted and cast into copper mold to get amorphous cylindrical rods with a diameter of 2 mm. The amorphism of the samples was confirmed by x-ray diffraction (XRD) using Rigaku D/max 2500 with Cu-Kα radiation.

Calorimetric measurements were performed on a differential scanning calorimetry apparatus (TA DSC Q200). Prior to the measurements, each sample was firstly heated to a specific temperature (T_g + 30 K, T_g is the glass transition temperature) at q = 20 K/min, held isothermally at the temperature for 180 s and then cooled down to ambient temperature at q = 20 K/min to ensure a known thermal history. The crystallized sample was obtained by annealing the amorphous sample at 520 K for 180 s and then cooling to the ambient temperature at q = 20 K/min.

Absolute specific heat capacity measurements of the glassy, crystalline and liquid states were carried out in conventional mode and temperature-modulated mode of DSC Q200, i.e. temperature-modulated DSC (TMDSC). More details about TMDSC are described in Ref. [15,16]. The underlying heating rate q, period t_p and amplitude A of the temperature oscillation were 3 K/min, 60 s and 0.5 K, respectively. Glass transition temperature and melting temperature of the alloys were measured in conventional mode of DSC Q200 at a standard heating rate of q = 20 K/min. To examine the heating rate dependence of glass transition temperature, a wide range of heating rate, q = 2–120 K/min, was adopted. In order to obtain accurate DSC data of the sample, identical measurements were performed on the empty pan as baseline to be subtracted from sample data and on the sapphire to get the calibration constant. The high purity nitrogen gas with a flow rate of 50 ml/min was purged into the DSC cell. The calorimeter was calibrated by indium standard.

* Corresponding author. Tel.: +86 10 82649085; fax: +86 10 82649533.
E-mail address: ghrao@aphy.iphy.ac.cn (G.H. Rao).

0925-8388/$ – see front matter © 2011 Elsevier B.V. All rights reserved.
doi:10.1016/j.jallcom.2011.01.106

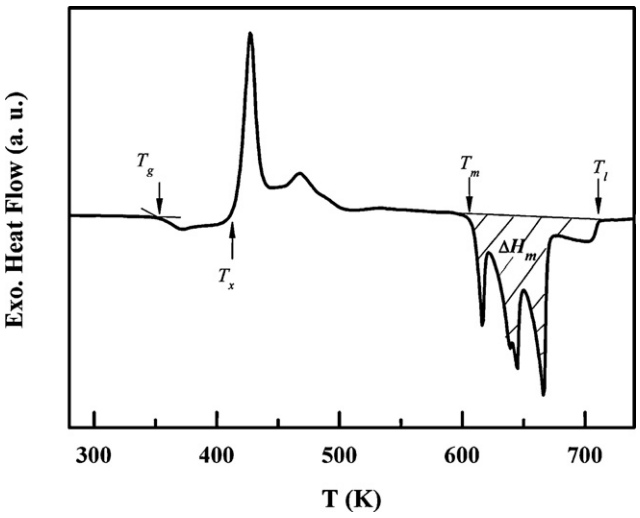

Fig. 1. DSC standard scan for $Ce_{68}Al_{10}Cu_{20}Co_2$ bulk metallic glass at heating rate $q = 20$ K/min. T_g is glass transition temperature, T_x the temperature of crystallization, T_m the melting temperature, T_l the liquidus temperature and ΔH_m the heat of melting.

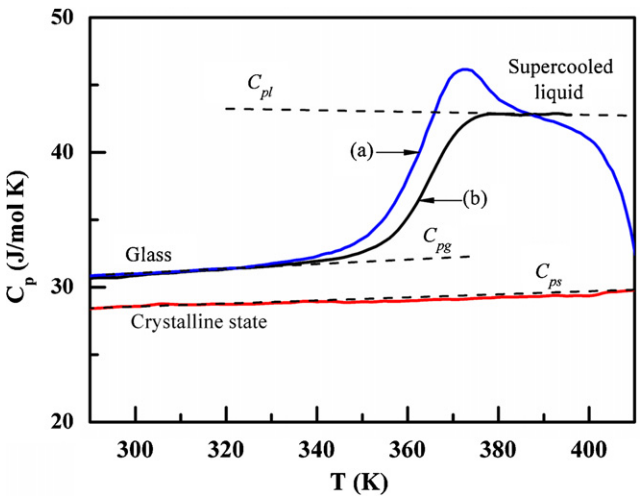

Fig. 2. Specific heat capacity of glass, supercooled liquid and crystalline for $Ce_{68}Al_{10}Cu_{20}Co_2$ alloy. (a) Specific heat capacity curve measured at standard heating rate $q = 20$ K/min; (b) specific heat capacity curve measured at $q = 3$ K/min, period $p = 60$ s, and $A = 0.5$ K. C_{pl}, C_{pg} and C_{ps} indicate the linear extrapolations of the specific heat capacity of supercooled, glass and crystalline, respectively (dash lines).

3. Results and discussion

3.1. Thermodynamic properties

DSC trace measured at the standard heating rate of 20 K/min is exemplified in Fig. 1 for $Ce_{68}Al_{10}Cu_{20}Co_2$ bulk metallic glass. The DSC trace manifests obviously the glass transition with an endothermic change, crystallization with exothermic peaks, and sequential melting with several large endothermic peaks. The characteristic temperatures such as the glass transition T_g, the crystallization temperature T_x, the melting temperature T_m and liquidus temperature T_l are given in Table 1 for all the investigated samples. The heat of melting ΔH_m determined by integrating the melting peaks is also listed in Table 1.

Fig. 2 shows the specific heat capacity of glass, supercooled liquid and crystalline of $Ce_{68}Al_{10}Cu_{20}Co_2$ alloy. The curves (a) and (b) were measured by standard DSC scanning at $q = 20$ K/min and TMDSC at $q = 3$ K/min, $p = 60$ s, and $A = 0.5$ K, respectively. As mentioned in Ref. [16], TMDSC is able to separate glass transition from the enthalpic relaxation and the crystallization. Therefore, the absolute specific heat capacity of supercooled liquid can be determined more accurately by TMDSC. The temperature dependence of specific heat capacity of glass (C_{pg}), supercooled liquid (C_{pl}), and the crystalline state (C_{ps}) for $Ce_{68}Al_{10}Cu_{20}Co_2$ alloy in the wide temperature range is deduced from the extrapolation of the available data. The temperature dependence of C_{pl}, C_{ps} and C_{pg} (in unit of J/mol K) was approximated by a linear form of $a + bT$ with $a = 45.1$, $b = -5.8 \times 10^{-3}$ for C_{pl}, $a = 25.1$, $b = 0.011$ for C_{ps} and $a = 23.7$, $b = 0.024$ for C_{pg}, respectively. Using the specific heat capacity difference $\Delta C_{pl\text{-}s} = C_{pl} - C_{ps}$, the heat of melting ΔH_m and the melting temperature T_m, the temperature dependence of thermodynamic functions of the Ce-based alloys can be derived. The enthalpy, entropy, and Gibbs free energy of supercooled liquid with respect to the crystalline state can be calculated by the equations:

$$\Delta H(T) = \Delta H_m + \int_{T_m}^{T} \Delta C_{pl-s}(T')dT' \quad (1)$$

$$\Delta S(T) = \Delta S_m + \int_{T_m}^{T} \left(\frac{\Delta C_{pl-s}(T')}{T'} \right) dT' \quad (2)$$

$$\Delta G(T) = \Delta H(T) - T\Delta S(T) \quad (3)$$

where ΔS_m is the entropy of melting that can be approximated as $\Delta H_m/T_m$. The calculated thermodynamic functions of the Ce-based alloys as a function of temperature are shown in Figs. 3–5, respectively. Both enthalpy and entropy decrease as temperature decreases. In Fig. 4, the entropy of the supercooled liquid is extrapolated down to the Kuazmann temperature (T_K), where the entropy of the supercooled liquid reaches the entropy of the crystalline state. Kauzmann declared that it was impossible for a supercooled liquid to exist below this temperature, so T_K is considered as the

Table 1
Glass transition temperature T_g, crystallization temperature T_x, melting temperature T_m, liquidus temperature T_l, heat of melting ΔH_m and Kauzmann temperature T_K for Ce-based alloys.

BMGs	T_g (K)	T_x (K)	T_m (K)	T_l (K)	ΔH_m (kJ/mol)	T_K (K)
$Ce_{68}Al_{10}Cu_{20}Co_2$	353	417	616	712	7.3	248
$Ce_{65}Al_{10}Cu_{20}Co_5$	365	426	614	705	7.2	250
$Ce_{60}Al_{10}Cu_{20}Co_{10}$	379	447	613	727	7.4	274

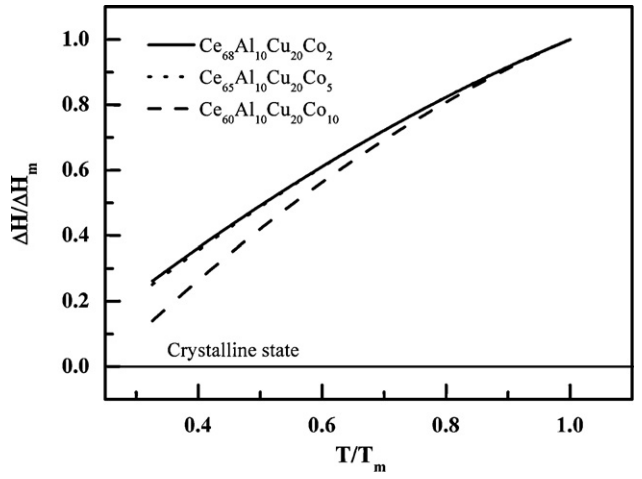

Fig. 3. The calculated enthalpy of the supercooled liquid of Ce-based alloys with respect to the crystalline state, normalized by heat of melting, ΔH_m.

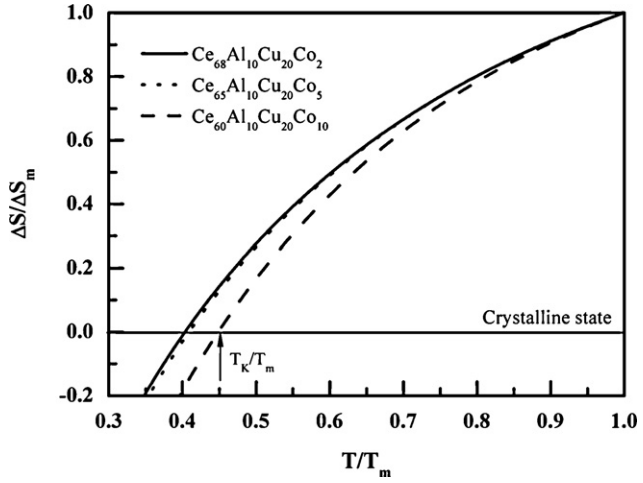

Fig. 4. The calculated entropy of the supercooled liquid of Ce-based alloys with respect to the crystalline state scaled by values at melting temperature. T_K is the extrapolated Kauzmann temperature, where $\Delta S/\Delta S_m = 0$.

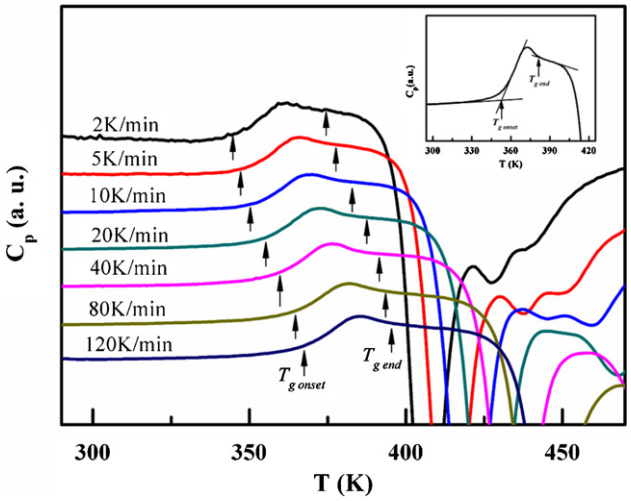

Fig. 6. DSC traces of $Ce_{68}Al_{10}Cu_{20}Co_2$ alloy at different heating rates (q = 2, 5, 10, 20, 40, 80, 120 K/min). The inset shows how to determine the interval temperature between the onset and the end glass transition temperatures.

low bound for glass transition due to the fact that the liquid could not have an entropy smaller than that of the crystalline [17]. The values of T_K of Ce-based alloys are listed in Table 1. However, it should be noted that the existence of Kauzmann temperature is still under debating as indicated in recent publications [18,19].

Fig. 5 shows the calculated Gibbs free energy with respect to the crystalline state for Ce-based alloy and for other bulk metallic glass-forming alloys [20]. Generally speaking, glass-forming ability (GFA), indicated by a low critical cooling rate, has an opposite relationship with the driving force for crystallization. The difference in Gibbs free energy between liquid and crystalline, ΔG, is the driving force for crystal nucleation and crystal growth [21]. The smaller the ΔG, the smaller the driving force of crystallization, and therefore the smaller nucleation and growth rate in the supercooled and the better glass-forming ability. This is consistent with the experimental results shown in Fig. 5, i.e. the smallest ΔG occurs for $Pd_{43}Ni_{10}Cu_{27}P_{20}$ alloy, which has the critical cooling rate of 1 K/s (indicated in plot), while the largest ΔG is for $Zr_{64}Ni_{34}$ with a critical cooling rate of 10^4 K/s.

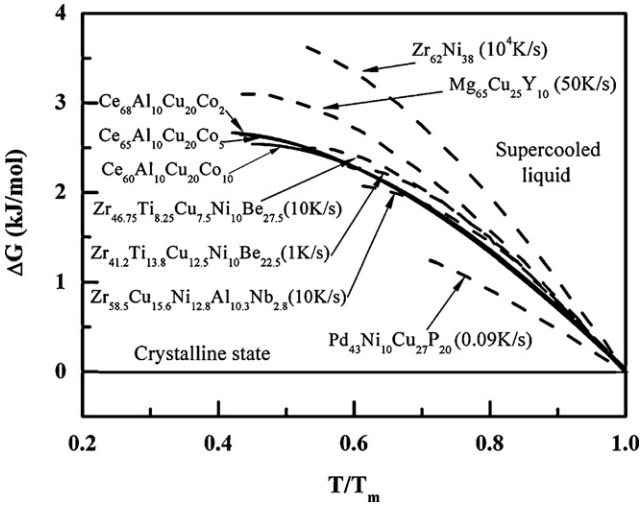

Fig. 5. Gibbs free energy of the supercooled liquid with respect to the crystalline state as a function of temperature for different glass-forming alloys. Solid lines: present work on the Ce-based BMGs. Dashed-lines: reported work on other BMGs for comparison.

For the investigated Ce-based alloys with good GFA, ΔG is similar and reaches ~2.7 kJ/mol at T_K. The value is comparable to that of the excellent glass former $Zr_{46.75}Ti_{8.25}Cu_{7.5}Ni_{10}Be_{27.5}$ which has the critical cooling rate of 10 K/s. Busch et al. [22] argued that the small value of ΔG was ascribed to the low entropy of fusion of these alloys, which implies that supercooled liquid has a small free volume and a highly random dense packing structure.

3.2. Kinetics

Glass transition from amorphous state to the supercooled liquid is investigated by DSC at different heating rates. Fig. 6 shows the DSC traces of $Ce_{68}Al_{10}Cu_{20}Co_2$ alloy measured at heating rates ranging from 2 K/min to 120 K/min. The onset glass transition temperature $T_{g\,onset}$ and end glass transition temperature $T_{g\,end}$ increase with increasing heating rate, indicating an evident kinetic behavior. As shown in the inset in Fig. 6, $T_{g\,onset}$ is taken to be the intersection point of baseline before transition and the maximum slope of specific heat capacity, and $T_{g\,end}$ is the intersection point of the baseline after transition and the minimum slope of specific heat capacity. Structural relaxation can be calorimetrically observed in temperature interval, $\Delta T_g = T_{g\,end} - T_{g\,onset}$ [23]. At a constant heating rate q, the average relaxation time τ can be defined as:

$$\tau = \frac{\Delta T_g}{q} \tag{4}$$

The temperature dependence of τ is usually described by Vogel–Fulcher–Tamman (VFT) equation [23]:

$$\tau = \tau_0 \exp\left(\frac{DT_0}{T - T_0}\right) \tag{5}$$

where D is a constant and T_0 is the VFT temperature at which relaxation time approaches infinity. The τ_0 refers to the infinite high temperature relaxation time. As $1/T \to 0$, $\tau_0 \propto N_A \cdot h/V$, where N_A is the Avogadro's constant, h the Planck's constant, and V the molar volume. In this work, the pre-exponential factor, τ_0, is set as a fixed value of 2×10^{-13} s [24]. The onset temperature $T_{g\,onset}$ is employed to approximate the temperature corresponding to τ [22]. Relaxation times determined by Eq. (4) are fitted with Eq. (5) using D and T_0 as fitting parameters. The parameters fitting best to the experimental data for the investigated alloys are listed in Table 2.

The relaxation dynamics of supercooled liquids are conventionally discussed in terms of the fragility proposed by Angell [25], which measures the degree of deviation from a simple Arrhenius

Table 2
The parameters fitting to the VFT equation and the fragility parameter m.

BMGs	D	T_0 (K)	m
$Ce_{68}Al_{10}Cu_{20}Co_2$	5440 ± 470	193 ± 14	32.6
$Ce_{65}Al_{10}Cu_{20}Co_5$	5300 ± 620	208 ± 18	34
$Ce_{60}Al_{10}Cu_{20}Co_{10}$	5440 ± 650	214 ± 19	34

behavior of the temperature dependence of the relaxation time. The fragility parameter is defined as $m = d \log \tau / d\,(T_g/T)|_{T=Tg}$. From Eq. (5) and the VFT fitting parameters, the fragility parameter m at T_g can be calculated by:

$$m = \frac{DT_0T_g}{(T_g - T_0)^2 \ln 10} \tag{6}$$

Fig. 7 displays the Angell fragility plot [25] for the Ce-based alloys and some typical glass-forming liquids in the vicinity of glass transition [3,26,27]. Among them, SiO_2 is the strongest glass former, while O-terphenyl is the most fragile glass former. The relaxation time is shown as a function of inverse temperature normalized by T_g^*, which is defined as the onset glass transition temperature measured at a heating rate of 1 K/min on the DSC. At this heating rate, the equilibrium viscosity at the onset of the corresponding T_g is close to 10^{12} Pa s [23]. For our investigated samples, the T_g^* can be obtained by extrapolating VFT curve to the relaxation time corresponding to 1 K/min. Fig. 7 shows that the Ce-based alloys exhibit the strong liquid behavior, even stronger than $Zr_{46.75}Ti_{8.25}Cu_{7.5}Ni_{10}Be_{27.5}$ (Vit4) alloy, the typical strong supercooled metallic alloys reported so far. Furthermore, the Ce-based BMGs corroborate the general knowledge that bulk metallic alloys have a fragility index in the range $30 < m < 70$ near T_g, i.e. intermediate between SiO_2 and O-terphenyl in the fragility plot [28]. Based on structure characterization and computer simulation, Sheng et al. [29] suggested that atoms in the strong liquid would be relatively densely packed and possess pronounced short or media range order, which results in a low enthalpy and entropy and slows down the crystallization kinetics.

3.3. Modeling

The phenomenological model, Tool–Narayanaswamy–Moynihan model [30–32], was used to model the structural relaxation of glass transition. It is well known that the structural relaxation response to a temperature change for amorphous materials is non-exponential and non-linear [33]. According to the TNM model, the Kohlrausch–Williams–Watt (KWW) stretched exponential function [34,35] can be chosen as the response function for a glass system not much far from equilibrium:

$$\phi(t) = \exp\left[-\left(\frac{t}{\tau}\right)^{\beta}\right] \tag{7}$$

where τ is the average relaxation time and β ($0 < \beta \leq 1$) expresses the extent of the non- exponentiality of the relaxation. A single relaxation time is denoted by $\beta = 1$. The non-linearity of structural relaxation process is incorporated into the TNM model by allowing the relaxation time to depend on particular structure of the supercooled liquid in addition to the temperature. So Tool [30] and Narayanaswamy [31] introduced a fictive temperature T_f as a structural parameter and gave an Arrhenius-like expression for τ:

$$\ln \tau = \ln \tau_0 + \frac{x\Delta h}{RT} + \frac{(1-x)\Delta h}{RT_f} \tag{8}$$

where τ_0 is the characteristic relaxation time, x ($0 < x \leq 1$) is the non-linearity parameter which partitions the dependence of τ on temperature and structure, Δh is the effective activation energy. Taking into account the non-Arrhenius property of relaxation in the supercooled liquid, the VFT-like expression for τ is used as follows:

$$\ln \tau = \ln \tau_0 + \frac{xD}{T - T_0} + \frac{(1-x)D}{T_f - T_0} \tag{9}$$

T_f is defined as the temperature at which the enthalpy extrapolated along the glassy line would equal that extrapolated along the supercooled liquid. Therefore, the fictive temperature evolves from actual temperature at equilibrium, $T_f = T$, to a constant value in the glassy state. Using Eq. (7) for an arbitrary thermal history starting initially in the equilibrium state, $T_f = T_a$, the initial temperature, the evolution of the fictive temperature can be calculated by numerical integration and expressed as:

$$T_{f,n} = T_a + \sum_{j=1}^{n} \Delta T_j \left\{1 - \exp\left[-\sum_{i=j}^{n}\left(\frac{\Delta t_i}{\tau_i}\right)^{\beta}\right]\right\} \tag{10}$$

where $T_{f,n}$ is the fictive temperature following nth temperature step, and ΔT_j is the temperature change at the jth time step, Δt_j. For any time step i, the relaxation time τ_k is taken from Eq. (9).

In order to compare the model with the experimental data, it is convenient to use TNM specific heat capacity defined as dT_f/dT [33]:

$$\frac{dT_f}{dT} = \frac{C_p(T) - C_{pg}(T)}{C_{pl}(T) - C_{pg}(T)} \tag{11}$$

where C_p is the observed specific heat capacity, C_{pg} and C_{pl} are the specific heat capacities for the liquid and the glass, respectively. In our experiment, C_p is the apparent specific heat capacity measured by conventional DSC scanning at $q = 20$ K/min (Fig. 2), while C_{pl} determined by TMDSC (Fig. 2) is used. The C_{pg} determined by the two methods is almost the same and the TMDSC result is adopted in the calculation. The fitting procedure was performed with Eq. (10) by optimizing parameters x and β, while keeping the values of τ_0, D and T_0 as constants. The values of D and T_0 obtained by VFT fitting mentioned above were used. Fig. 8 shows plots of dT_f/dT versus temperature derived from the measured DSC data and the TNM model fitting results for the three investigated samples. The model provides a reasonable approximation for the experimental behavior. The values of x and β for Ce-based alloys and other glass formers are listed in Table 3. As shown in Table 3, the values of x and β are not sensitive to the content of Co in the Ce-based alloys investigated. Comparing to other type of glass formers (inorganic glasses and polymers), the nonlinear parameter x for BMGs glass-forming alloys is approximately a constant. It can be understood

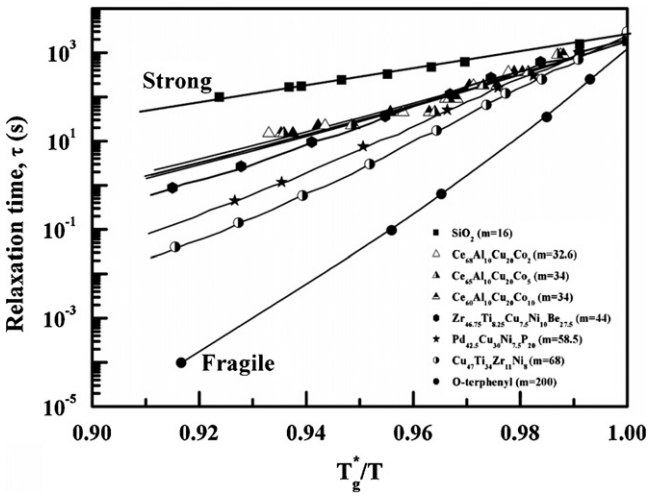

Fig. 7. The Angell plot to compare relaxation time of Ce-based alloys with other glass formers. The Angell fragility parameter m of each BMG is indicated.

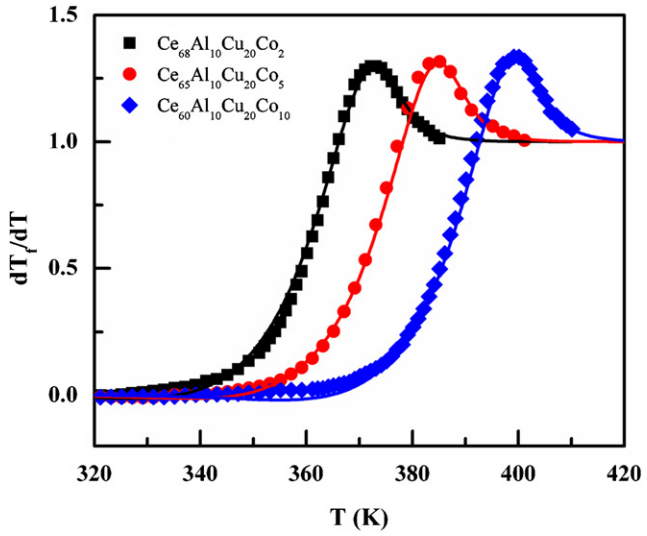

Fig. 8. dT_f/dT as a function of temperature obtained from DSC data at heating rate of 20 K/min after cooling at the same rate for Ce-based alloys. The solid lines through the data were calculated from TNM model using the parameters given in Tables 2 and 3.

Table 3
TNM parameters for different glass formers.

Glass	x	β	Ref.
$Ce_{68}Al_{10}Cu_{20}Co_2$	0.53	0.6	This work
$Ce_{65}Al_{10}Cu_{20}Co_5$	0.5	0.6	This work
$Ce_{60}Al_{10}Cu_{20}Co_{10}$	0.53	0.63	This work
$Zr_{65}Al_{10}Ni_{10}Cu_{15}$	0.53	0.79	[36]
$Zr_{46.75}Ti_{8.25}Cu_{7.5}Ni_{10}Be_{27.5}$	0.55	0.5	[37]
PVC	0.1	0.23	[32]
BPAPC	0.19	0.46	[32]
ZBLAN	0.35	0.56	[32]
PS	0.46	0.71	[32]
NBS711	0.65	0.65	[32]
B_2O_3	0.4	0.65	[32]
$40Al\text{-}60Ag_2MoO_4$	0.5	–	[32]
$NaKSi_3O_7$	0.7	0.66	[38]

based on Eq. (8) that the nonlinear parameter x can be viewed as a measure of relative contribution of temperature and microstructure defined by T_f to the average relaxation time. The similarity of the nonlinearity of structural relaxation in metallic glasses may originate from the similar packing structure of metallic supercooled liquids, whereas other types of glass formers such as polymers have more complex and flexible structures, leading to a large change in x. The value of $\beta \approx 0.61$ for Ce-based alloys is comparable to those reported for other metallic glasses and other types of glasses, and $\beta < 1$ is indicative of a broad distribution of the relaxation time originating from the dynamical heterogeneity of the microstructure, which is an intrinsic property of the glass transition [39].

4. Summary

The thermodynamic and kinetic properties of $Ce_{68}Al_{10}Cu_{20}Co_2$, $Ce_{65}Al_{10}Cu_{20}Co_5$, and $Ce_{60}Al_{10}Cu_{20}Co_{10}$ alloys were studied by calorimetric measurements. The specific heat capacity of supercooled liquid was obtained by TMDSC. Thermodynamic functions, such as enthalpy, entropy and Gibbs free energy, are calculated as a function of temperature. The small value of Gibbs free energy difference between the supercooled liquid and the crystalline state of Ce-based alloys at Kauzmann temperature could be one of the important factors for their high glass-forming ability. The kinetics can be probed by heating rate dependence of glass transition temperature of Ce-based alloys. The fragility of the alloys was derived from the parameters of VFT equation. The Ce-based alloys exhibit a strong liquids character, even stronger than Vit4, one of the typical strong liquids in the BMGs. The strong liquid behavior means a sluggish kinetics in the supercooled liquid with low atomic mobility, which retards the nucleation of crystals from a homogeneous liquid [22]. Therefore, both thermodynamic and kinetic factors can contribute to the excellent glass-forming ability of the Ce-based alloys.

The TNM model extended by VFT equation describes well the structural relaxation of Ce-based alloys in the glass transition region. The nonlinearity parameter x derived from the TNM model fitting to the experimental calorimetric data is insensitive to the composition of alloys investigated and is very close to that of other metallic glass-forming liquids. The $\beta \approx 0.61 < 1$ for Ce-based alloys suggests a broad distribution of the relaxation time.

Acknowledgements

This work is financially supported by the National Natural Science Foundation of China (Grants no. 10774166, no. 50631040) and the National Basic Research Program of China (Grant no. 2006CB601101, no. 2006CB605101). We thank K. Zhao for the help in experiments.

References

[1] A. Inoue, Acta Mater. 48 (2000) 279–306.
[2] W.L. Johnson, MRS Bull. 24 (1999) 42–56.
[3] R. Busch, W.L. Johnson, Appl. Phys. Lett. 72 (1998) 2695–2697.
[4] G.J. Fan, J.F. Löffler, R.K. Wunderlich, H.J. Fecht, Acta Mater. 52 (2004) 667–674.
[5] D.J. Wang, Y.J. Huang, J. Shen, J. Non-Cryst. Solids 355 (2009) 986–990.
[6] G. Fiore, L. Battezzati, J. Alloys Compd. 483 (2009) 54–56.
[7] L. Battezzatia, G.M. Mortarino, J. Alloys Compd. 483 (2009) 222–226.
[8] L. Battezzati, A. Habib, D. Baldissin, P. Rizzi, J. Alloys Compd. 504S (2010) S48–S51.
[9] A.H. Caia, W.K. Ana, Y. Luo, T.L. Li, X.S. Li, X. Xiong, Y. Liu, J. Alloys Compd. 490 (2010) 642–646.
[10] T.A. Basera, J. Dasb, J. Eckertb, M. Baricco, J. Alloys Compd. 483 (2009) 146–149.
[11] B. Zhang, W.H. Wang, Appl. Phys. Lett. 85 (2004) 61–63.
[12] B. Zhang, D.Q. Zhao, M.X. Pan, W.H. Wang, Acta Mater. 54 (2006) 3025–3032.
[13] B. Zhang, D.Q. Zhao, M.X. Pan, W.H. Wang, A.L. Greer, Phys. Rev. Lett. 94 (2005) 1–4, 205502.
[14] B. Zhang, D.Q. Zhao, M.X. Pan, W.H. Wang, J. Non-Cryst. Solids 352 (2006) 5687–5690.
[15] M. Reading, Trends Polym. Sci. 1 (1993) 248–253.
[16] M. Reading, D.J. Hourston, Modulated Temperature Differential Scanning Calorimetry: Theoretical and Practical Application in Polymer Characterization, Springer, Netherlands, 2006.
[17] W. Kauzmann, Chem. Rev. 43 (1948) 219–256.
[18] T. Hecksher, A.I. Nielsen, N.B. Olsen, J.C. Dyer, Nat. Phys. 4 (2008) 737–741.
[19] J.C. Mauro, Y.Z. Yue, A.J. Ellison, P.K. Gupta, D.C. Allan, Proc. Natl. Acad. Sci. U.S.A. 106 (2009) 19780–19784.
[20] R. Busch, J. Schroers, W.H. Wang, MRS Bull. 32 (2007) 620–623.
[21] H.J. Fecht, W.L. Johnson, Mater. Sci. Eng. A 375 (2004) 2–8.
[22] R. Busch, Y.J. Kim, W.L. Johnson, J. Appl. Phys. 83 (1998) 4134–4141.
[23] R. Busch, E. Bakke, W.L. Johnson, Acta Metall. Mater. 46 (1998) 4725–4732.
[24] S.V. Nemilov, Glass Phys. Chem. 21 (1995) 91–95.
[25] C.A. Angell, Science 267 (1995) 1924–1935.
[26] S.C. Glade, W.L. Johnson, J. Appl. Phys. 87 (2000) 7249–7251.
[27] N. Nishiyama, A. Inoue, Appl. Phys. Lett. 80 (2002) 568–570.
[28] D.N. Perera, J. Phys.: Condens. Matter 11 (1999) 3807–3812.
[29] H.W. Sheng, W.K. Luo, F.M. Alamgir, J.M. Bai, E. Ma, Nature 439 (2006) 419–425.
[30] A.Q. Tool, J. Am. Ceram. Soc. 29 (1946) 240–253.
[31] O.S. Narayanaswamy, J. Am. Ceram. Soc. 54 (1971) 491–498.
[32] C.T. Moynihan, A.J. Easteal, M.A. DeBolt, J. Tucker, J. Am. Ceram. Soc. 59 (1976) 12–21.
[33] I.M. Hodge, J. Non-Cryst. Solids 169 (1994) 211–266.
[34] R. Kohlrausch, Ann. Phys. Chem. 72 (1847) 393.
[35] G. Williams, D.C. Watts, Trans. Faraday Soc. 66 (1970) 80.
[36] S.W. Martin, J. Walleser, A. Karthikeyan, D. Sordelet, J. Non-Cryst. Solids 349 (2004) 347–354.
[37] P. Wen, Z.F. Zhao, W.H. Wang, Sci. China Ser. G 51 (2008) 356–364.
[38] I.M. Hodge, Macromolecules 20 (1987) 2897–2908.
[39] H. Sillescu, J. Non-Cryst. Solids 243 (1999) 81–108.